ACS OMEGA

http://pubs.acs.org/journal/acsodf

Article

Theoretical Study of Anisotropic Carrier Mobility for Two-Dimensional Nb_2Se_9 Material

You Kyoung Chung, Junho Lee, Weon-Gyu Lee, Dongchul Sung, Sudong Chae, Seungbae Oh, Kyung Hwan Choi, Bum Jun Kim, Jae-Young Choi,* and Joonsuk Huh*

Cite This: *ACS Omega* 2021, 6, 26782−26790

Read Online

ABSTRACT: Finding new materials with satisfying all the desired criteria for nanodevices is an extremely difficult work. Here, we introduce a novel Nb_2Se_9 material as a promising candidate, capable of overcoming some physical limitations, such as a suitable band gap, high carrier mobility, and chemical stability. Unlike graphene, it has a noticeable band gap and no dangling bonds at surfaces that deteriorate transport properties, owing to its molecular chain structure. Using density functional theory (DFT) calculations with deformation potential (DP) theory, we find that the electron mobility of 2D Nb_2Se_9 across the axis direction reaches up to 2.56×10^3 cm^2 V^{-1} s^{-1} and is approximately 2.5−6 times higher than the mobility of other 2D materials, such as MoS_2, black phosphorous, and InSe, at room temperature. Moreover, the mobility of 2D Nb_2Se_9 is highly anisotropic ($\mu_a/\mu_c \approx 6.5$). We demonstrate the potential of 2D Nb_2Se_9 for applications in nanoscale electronic devices and, possibly, mid-infrared photodetectors.

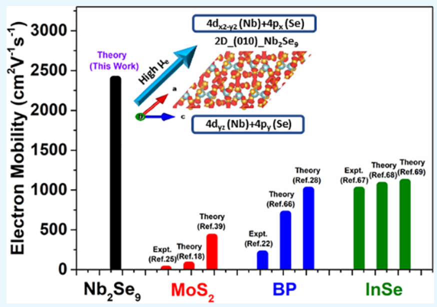

INTRODUCTION

Since the discovery of graphene in 2004,[1] successful isolation of individual atomic layers from bulk crystals using mechanical exfoliation has led to a considerable exploration of two-dimensional (2D) van der Waals (vdW) materials. The unique ballistic transport and extraordinarily high carrier mobility of graphene makes it suitable for various potential applications.[2−10] However, the major hurdle presented by its zero band gap motivates the exploration of other 2D vdW materials, including graphdiynes,[11,12] molybdenum disulfide (MoS_2),[13−19] molybdenum diselenide ($MoSe_2$),[20] tungsten disulfide (WS_2),[21] and black phosphorous (BP),[22−24] as promising materials for field-effect transistors (FETs) and highly sensitive photodetectors. While these materials have shown great potential for a wide range of chemical and physical applications, some limitations, due to inherent weaknesses, still persist. For example, MoS_2 has a moderate band gap (1.3−1.8 eV) but exhibits one order of magnitude lower mobility than the theoretically predicted phonon-limited value (400 cm^2 V^{-1} s^{-1}),[25] limiting its application in nanoelectronics. Phosphorene exhibits high carrier mobility (200−1000 cm^2 V^{-1} s^{-1})[26] and has a band gap of 0.3−2.0 eV, depending on its thickness, and this widely tunable band gap is promising for near- and mid-infrared (IR) optoelectronics.[27,28] Despite these excellent intrinsic material qualities, its instability in ambient air presents a fundamental challenge for practical utilization.[29,30] Therefore, significant efforts have been devoted to exploring 2D materials that satisfy the fundamental properties (finite band gap, high mobility, good stability, and the absence of surface dangling bonds), providing compatibility with quasi-2D conducting channels for future applications in nanoelectronics. Recently, a novel one-dimensional (1D) semiconducting Nb_2Se_9 material was synthesized in bulk *via* simple vapor transport.[31] The as-grown, needle-like, single crystal Nb_2Se_9 was formed by multiple single molecular chains coupled by weak vdW interactions,[32,33] and the experiment[34,35] showed that this bundle of chains could be easily separated by mechanical cleavage, as demonstrated by Novoselov *et al.*[36] The isolated Nb_2Se_9 flakes exhibited a quasi-2D layered structure, eventually to the monolayer, with thicknesses controlled by the repeated peeling method. The monolayer was stable with the uniform width of less than 1 nm, even though the exfoliation and analysis processes were performed under atmospheric conditions.[34] Moreover, Nb_2Se_9 nanowire was also stable in liquid exfoliation with various chemical environments such as water, PBS buffer solution, and organic solvents.[35,37] Therefore, it could be studied for the applications as a biomaterial[38] and an electrocatalyst.[39] With its characteristic molecular-chain structures, this Nb_2Se_9 material has no surface dangling bonds that function as scattering centers,[9] adversely affecting carrier transport properties when downscaled to less than a few tens of nanometers. Moreover, our previous theoretical study showed that Nb_2Se_9 materials, in 1D, 2D, and 3D structures,

Received: August 17, 2021
Accepted: September 20, 2021
Published: October 3, 2021

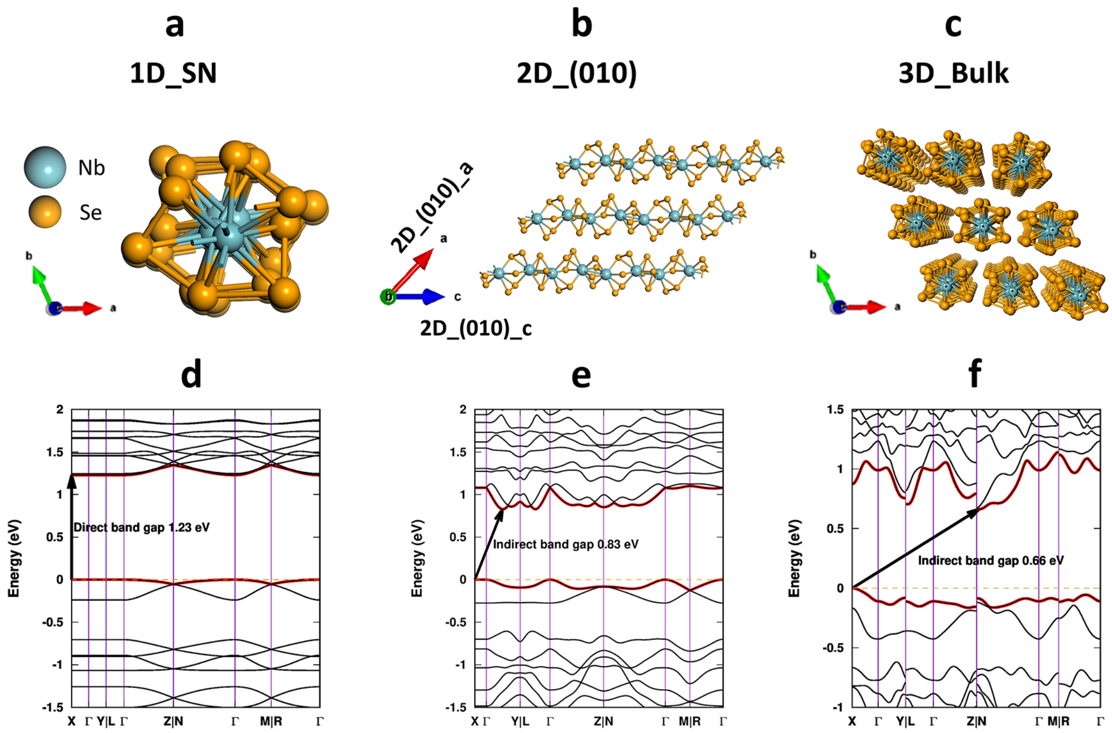

Figure 1. Atomic structures of the (a) 1D_SN, (b) 2D_(010) plane, and (c) 3D_bulk Nb_2Se_9 materials (gray and yellow spheres represent Nb and Se atoms, respectively). Electronic band structures of (d) 1D_SN, (e) 2D_(010) plane, and (f) 3D_bulk Nb_2Se_9 materials.

had nonzero band gaps in the range of 0.66−1.33 eV, depending on their structural dimensions, accompanied by an indirect-to-direct band gap transition from bulk crystal to single nanowire (SN) structures.[40] Additionally, high electron mobility is predicted, up to 10^3 cm^2 V^{-1} s^{-1} in 2D Nb_2Se_9 materials, across the axis direction using density functional theory (DFT) calculations. Electron mobility of 2D Nb_2Se_9 is highly anisotropic ($\mu_a/\mu_c \approx 6.5$) and approximately 2.5−6 times higher than that of other 2D materials, such as MoS_2, BP, and InSe, at room temperature. In addition, 2D Nb_2Se_9 has an appropriate band gap of 0.83 eV, important for telecommunication and solar energy harvesting applications.[28] These properties make Nb_2Se_9 potentially useful for practical applications in transistors,[41−44] solar cells,[23] photodetectors,[24] and thermoelectric devices.[45−47] Our proposed novel Nb_2Se_9 material is a promising candidate for overcoming the carrier transport deterioration commonly observed in 2D layered materials.

■ COMPUTATIONAL METHODS

Numerical Methods on Mobility Anisotropy. To understand the electronic and charge-transport properties of Nb_2Se_9 with structural dimension, we calculated the intrinsic carrier mobility based on the deformation potential (DP) theory, proposed by Bardeen and Shockley[48] in the 1950s to describe charge transport in nonpolar semiconductors. In an inorganic semiconductor, electron coherence is close to the acoustic phonon wavelength, which is much longer than bond length. Thus, scattering of a thermal electron or hole arises mostly from the acoustic phonons. Since Tang *et al.*[49] calculated oligoacene mobilities using acoustic phonon scattering, the DP theory has been widely used to evaluate charge transport in 1D nanoribbons,[11,12,18,19] 2D materials,[10,17,23,50] and 3D materials such as deoxyribonucleic acid stacks[51] and closely packed molecular crystals.[52] The DP approach can be simplified to an effective mass approximation, which we proved was valid for our system using a numerical derivation by Beleznay *et al.*[51,53] In our theoretical calculations, the elastic modulus and effective mass were found to be anisotropic in the 2D layered structure. Thus, we investigated the essential factors of DP parameters (elastic constant, deformation constant, and effective mass), which primarily influence mobility anisotropy, by applying two different numerical equations.(Tables S1 and S2) One only includes the influence of effective mass on mobility anisotropy as presented below (eqs 2 and 3),[54,55] and the other embraces the anisotropic properties of all three DP parameters, using eqs 4 and 5 of the Supporting Information. This comparison exhibits no noticeable difference (less than 7%) for carrier mobilities calculated with the two different equations, so we determine that the different effective mass in each direction and deformation potential are essential factors, affecting the mobility anisotropy. In other words, the anisotropic carrier mobility of Nb_2Se_9 material is determined by the complex influences of the three DP parameters, but anisotropy of the effective mass is more influential than that of the deformation potential. Therefore, we focused on the equations that apply the anisotropy of effective mass with the deformation potential fixed as an isotropic value for the 1D_SN, 2D_sheet, and 3D_bulk structures on mobility anisotropy, using the equations denoted as each dimension of the structure and the carrier transport direction. For 1D_SN, we only consider the main direction of the carrier movement as a nanowire direction, so the isotropic equation is applied to calculate the intrinsic carrier mobility. The following list of summarized equations employed for 1D_SN (eq 1), 2D_ sheet (eqs 2 and 3), and 3D_bulk structures (eqs 4 and 5, SI), using the DP approach to calculate the intrinsic carrier mobility:

https://doi.org/10.1021/acsomega.1c03728
ACS Omega 2021, 6, 26782−26790

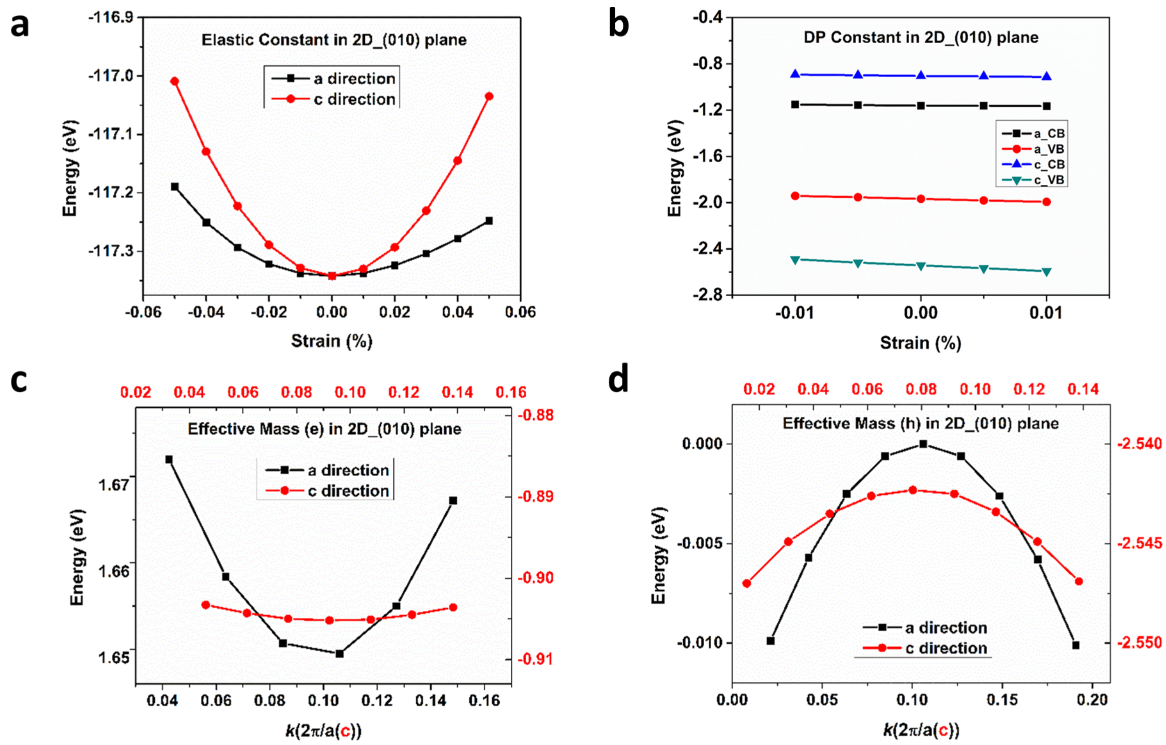

Figure 2. DP parameters using the HSE06 DFT functional. (a) Total unit cell energies of the 2D_(010) plane as a function of lattice deformation along the uniaxial direction (elastic constants can be obtained using a parabola fitting). (b) Shifts in the CBs and VBs of the 2D_(010) plane under uniaxial strain along the *a* and *c* directions. (c, d) Energy-strain relationships for the electron and hole effective masses for 2D_(010) along the (c) *a* and (d) *c* directions.

$$\mu_{1D\_c} = \frac{e\tau}{m^*} = \frac{e\hbar^2 C(1D\_c)}{(2\pi k_B T)^{1/2} |m_c^*|^{3/2} E_{1c}^2} \quad (1)$$

$$\mu_{2D\_a} = \frac{e\tau}{m^*} = \frac{e\hbar^3 C(2D\_a)}{k_B T |m_a^*|^{3/2} |m_c^*|^{1/2} E_{1a}^2} \quad (2)$$

$$\mu_{2D\_c} = \frac{e\tau}{m^*} = \frac{e\hbar^3 C(2D\_c)}{k_B T |m_a^*|^{1/2} |m_c^*|^{3/2} E_{1c}^2} \quad (3)$$

$$\mu_{3D\_c} = \frac{e\tau}{m^*} = \frac{2^{3/2}\pi^{1/2} e\hbar^4 C(3D\_c)}{3(k_B T)^{3/2} |m_a^*|^{1/2} |m_b^*|^{1/2} |m_c^*|^{3/2} E_{1c}^2} \quad (4)$$

where m^* is effective mass; τ is relaxation time; T is temperature; E_1 is the DP constant, which represents the strain-induced shift of the band edges; and C is the elastic modulus, attributed to simulation of lattice distortion by the strain. In anisotropic semiconductors, electrons and phonons behave differently in different directions, so the three-half exponent is applied to the directions in which an effective mass is expected to travel.

DFT Calculations. To obtain the intrinsic carrier mobility for 1D, 2D, and 3D Nb_2Se_9 structures with mobility anisotropy, we conducted DFT calculations with the projector-augmented wave method,[56] implemented in the Vienna ab-initio simulation package (VASP).[57] The ionic and electronic relaxations were carried out with the Perdew−Burke−Ernzerhof (PBE) generalized gradient approximation (GGA).[58] We adopted Grimme's DFT-D3 vdW corrections to include weak vdW interactions between Nb_2Se_9 chains. A hybrid HSE06[59] DFT functional was used to verify more elaborate band structures, but no prominent difference was found in mobility upon changes in structural dimensions. The energy cutoff was set to 520 eV. Gaussian smearing with Blöchl correction was used for geometry optimization, with a smearing width of 0.05 eV.

To describe the finite isolated nanowire, we placed nanowires in a triclinic unit cell with a vacuum spacing of 15 Å in the *x*- and *y*-directions to limit interwire interactions. The convergence criterion of the total energy in the self-consistent field iteration was 10^{-8} eV, whereas the maximum force allowed on each atom was 0.01 eV/Å. In self-consistent potential and total energy calculations, the Brillouin zone was sampled by a 1 × 1 × 6 grid for 1D_SN, 6 × 1 × 6 grid for the 2D_(010) plane, and 6 × 6 × 6 grid for the 3D_bulk in the Γ-centered automatic *k*-meshes scheme. The crystal orbital Hamiltonian population (COHP)[60,61] was used to analyze orbital energies and interactions between specific atoms.

RESULTS AND DISCUSSION

Geometry and Band Structure. We performed DFT calculations to investigate atomic and electronic properties of Nb_2Se_9 materials, as shown in Figure 1. The optimized geometries of the 1D_SN, 2D_(010) plane, and 3D_bulk Nb_2Se_9 materials are shown in Figure 1a−c. The unit cell of bulk Nb_2Se_9 has 4 niobium (Nb) cations and 18 selenium (Se) anions, forming a chain structure. The inorganic bulk crystals of Nb_2Se_9 are formed by strong bonds along the chain axis and weak interchain interactions across the chain axis. There are three distinct 2D sheets in the (010), (100), and (−101) planes, which can be formed by properly arranging 1D Nb_2Se_9 chains, depending on the cutting planes of the bulk Nb_2Se_9 structure.[62] We verified the stability of each plane by the phonon dispersion bands of the 2D-Nb_2Se_9 structure (Figure

https://doi.org/10.1021/acsomega.1c03728
ACS Omega 2021, 6, 26782−26790

Table 1. Various Parameters along the Lattice Constant (a or c) Direction for the 1D_SN, 2D_(010) Plane, and 3D_bulk Structures of the vdW Nb_2Se_9 Material, Calculated Using the PBE-D3 Functional (Numbers in Parenthesis Denote the Equation Number Used for Mobility Calculations)

	L (Å)	carrier type	C_{1D} (J/m)	C_{2D} (N/m)	C_{3D} (N/m^2)	E_{1a} (eV)	E_{1c} (eV)	m_a* (m$_e$)	m_b* (m$_e$)	m_c* (m$_e$)	μ (cm^2 V^{-1} s^{-1})
1D_c (eq 1)	13.0	e	2.61×10^{-8}				−1.19			1.22	4.19×10
		h	2.61×10^{-8}				−2.33			−4.49	0.25×10
2D_a (eq 2)	8.2	e		14.8		−0.94		0.29		1.43	1.91×10^3
		h		14.8		−2.63		−1.35		−1.04	2.85×10
2D_c (eq 2)	13.0	e		38.5			−1.72	0.29		1.43	3.01×10^2
		h		38.5			−4.97	−1.35		−1.04	2.69×10
3D_c (eq 3)	13.2	e			9.58×10^{10}		−6.69	0.41	1.47	1.37	1.04×10^2
		h			9.58×10^{10}		−10.05	−1.25	−2.32	−0.43	1.19×10^2

Table 2. Various Parameters along the Lattice Constant (a or c) Direction for the 1D_SN, 2D_(010) Plane and 3D_bulk vdW Nb_2Se_9 Materials, Calculated Using the Hybrid HSE06 Functional (Numbers in Parenthesis Denote the Equation Number Used for Mobility Calculations)

	L (Å)	carrier type	C_{1D} (J/m)	C_{2D} (N/m)	C_{3D} (N/m^2)	E_{1a} (eV)	E_{1c} (eV)	m_a* (m$_e$)	m_b* (m$_e$)	m_c* (m$_e$)	μ (cm^2 V^{-1} s^{-1})
1D_c (eq 1)	13.0	e	2.61×10^{-8}				1.06			1.56	5.94×10
		h	2.61×10^{-8}				−2.74			−6.64	0.10×10
2D_a (eq 2)	8.2	e		14.8		−0.73		0.31		1.80	2.56×10^3
		h		14.8		−2.83		−1.44		−1.21	2.07×10
2D_c (eq 2)	13.0	e		38.5			−1.30	0.31		1.80	3.60×10^2
		h		38.5			−5.06	−1.44		−1.21	2.03×10
3D_c (eq .3)	13.2	e			9.58×10^{10}		−6.50	0.35	1.21	1.31	1.39×10^2
		h			9.58×10^{10}		−10.60	−1.16	−1.27	−0.51	1.18×10^2

S1)[62,63] The (010) plane is the most stable, and the other planes have 0.21 eV higher energy than the plane (010). We chose the (010) plane for the 2D Nb_2Se_9 sheets as the most stable structure, and the two directions (denoted as 2D_(010)_a and 2D_(010)_c) were considered for carrier mobility, as presented in Figure 1b. Electronic structures of the 1D_SN, 2D_(010) plane, and 3D_bulk Nb_2Se_9 materials are shown in Figure 1d−f, respectively. Compared to valleys of the valence band (VB) and conduction band (CB) in the 2D_(010) plane and 3D_bulk, those in 1D_SN have broader, almost flat shapes, which reduce electron effective mass and mobility. The 2D_sheets and 3D_bulk Nb_2Se_9 structures are indirect band gap semiconductors with band gaps of 0.83 and 0.66 eV, respectively. 1D_SN has a 1.23 eV direct band gap at the X point, as determined by the PBE-D3 DFT functional, and the band gap of 3D_bulk Nb_2Se_9 structures is shifted to a larger band gap (1.43 eV) by the HSE06 hybrid functional (Figure S2). The indirect-to-direct band gap transition of Nb_2Se_9 upon structural dimension renders this material suitable for FET applications.

DP Constants. In this study, we conducted DFT calculations based on the DP theory because we only considered the acoustic phonon scattering mechanism. The acoustic phonon wavelength is much longer than bond length in our Nb_2Se_9 material. DP constants include the elastic constant (C), deformation constant (E_1), and effective mass (m_e*). The analytical methods used to obtain the DP constants for the 2D_(010) plane of a Nb_2Se_9 sheet are shown in Figure 2a−d. Figure 2a shows variations in total energy (E) with the uniaxial strain (δ) applied along the lattice directions (a and c) in the 2D_(010) plane for a Nb_2Se_9 sheet. The elastic modulus is defined as $C_{2D} = [\partial^2 E/\partial\delta^2]/\Delta$, where E is the total energy of the unit cell, δ is the uniaxial strain applied along the lattice direction, and $\Delta = S/S_0$ describes the change in surface area at a dilation. The elastic constant C is obtained by parabola fitting energy-strain curves, and the value of C_{3D} in a 3D structure is obviously higher than that of C_{1D} in a 1D structure. This implies that the elastic modulus is proportional to mobility. On the other hand, the elastic modulus of C_{2D} in the 2D_(010)_c direction is approximately 2.5 times greater than that of C_{2D} in the 2D_(010)_a direction. This shows the inverse relationship between elastic constant and carrier mobility, motivating us to evaluate other parameters associated with high carrier mobility. Figure 2b shows band edge shifts as a function of uniaxial strain. By dilating the lattice, we calculated the DP constant E_1 as $dE/d\delta$, which is equivalent to the slope of the fitting line with five points, where E is the energy of the CB edge for the electron and VB edge for the hole under uniaxial strain (δ) applied along the lattice direction. When the lattice is dilated, due to applied strain along the uniaxial direction, these energy band edges shift because of the interaction between the electrons (thermal energy) and acoustic modes (vibration).[64] Considering dilations in the longitudinal waves, carrier mobility is related to shifts in the CB and VB. For a Nb_2Se_9 sheet, the VB edge energy is more deformed than the CB edge energy under strain, so hole mobility is expected to be lower than electron mobility. Figure 2c,d shows the energy-strain relationships along the lattice direction. The effective mass, m*, is calculated using $\hbar^2[\partial^2\varepsilon(k)/\partial k^2]^{-1}$, where $\varepsilon(k)$ is the band energy at the minimum valley for the electron and maximum peak for the hole along the k-point. For parabolic bands, the electron will move much like a free particle with m*, which results in constant effective masses. Using this parabolic approximation,[65] we see that the effective carrier masses are parabolic in the 2D_(010) plane in each direction, allowing us to apply the DP theory in our calculations. Indicating that the effective mass is inversely proportional to band curvature, the more parabolic band shape for the 2D_(010)_a direction is expected to have a smaller effective mass, contributing to its higher carrier mobility.

https://doi.org/10.1021/acsomega.1c03728
ACS Omega 2021, 6, 26782−26790

Intrinsic Carrier Mobility. Based on the obtained energy band spectrum using the VASP program, the acoustic-phonon-limited mobility at room temperature (300 K) was obtained with values E_1, C, and m^*. The results are tabulated in Tables 1 and 2 for the PBE-D3 and the HSE06 DFT functionals, respectively. In our calculations, electron mobility in 1D and 2D structures is obviously higher than hole mobility, whereas electron mobility in the 3D structure is on nearly the same order of magnitude as hole mobility. Our results show that the Nb_2Se_9 material exhibits high electron mobility, especially in the 2D_(010)_ plane along the *a* direction, which is approximately 40 times higher than the 1D structure and highly anisotropic ($\mu_a/\mu_c \approx 6.5$). This highly anisotropic electron mobility in the 2D_(010)_*a* direction originates from the smaller DP constant (−0.94 eV) and lower effective mass (0.31 m_e), compared to the bigger DP constant (−2.63 eV) and higher effective mass (0.80 m_e) in the 2D_(010)_*c* direction. In addition, the 3D_bulk along *a* direction also shows the anisotropic electron mobility ($\mu_a/\mu_c \approx 0.6$), using the PBE-D3 functional, as presented in Table S1. In particular, electron mobility in the 2D_(010)_*a* plane reached 2.56×10^3 $cm^2\ V^{-1}\ s^{-1}$ (HSE06) using eq 2 and only showed a difference of less than 7% for carrier mobilities, calculated by eqs 4 and 5 of the Supporting Information. From this fact, we discover that effective mass and the deformation potential are more influential factors on mobility anisotropy in 1D, 2D, and 3D structures, even if carrier mobility, based on the DP theory, is determined by the complex interplay of three DP constants.

In Figure 3, the proposed 2D Nb_2Se_9 material shows high carrier mobility compared to other 2D materials currently used in nanoelectronics. This graph clearly shows that the electron mobility of Nb_2Se_9 in the 2D_(010)_*a* direction is approximately six times higher than the highest mobility of MoS_2 (10−400 $cm^2\ V^{-1}\ s^{-1}$),[18,25,42] 2.5 times higher than that of BP (200−1000 $cm^2\ V^{-1}\ s^{-1}$),[22,28,66,67] and 2.3 times higher than that of InSe (1000−1100 $cm^2\ V^{-1}\ s^{-1}$).[68−70] Carrier mobility is an essential property for any semiconducting material, especially those used in FETs. Carrier density and mobility determine the controllable switching of conductance of a semiconducting channel in the operation of electronic devices.[28] So far, semiconductor devices have achieved improved performance,[71,72] reduced power consumption, and improved integration through scaling down. However, issues of carrier velocity saturation[73,74] and threshold voltage reduction still need to be addressed, owing to the reduction in channel length, which is a limiting factor for scaled down processes below 100 nm. Many problems have occurred, and various methods are being studied, though not in universal scaling. In the case of the proposed 2D Nb_2Se_9 material, the structure is formed by 1D chains, eliminating dangling bonds at the surfaces, and providing high electron mobility. Therefore, given its characteristic properties, the proposed vdW Nb_2Se_9 material is a potential alternative material, capable of solving the above-mentioned problems for nanoscale electronic devices.

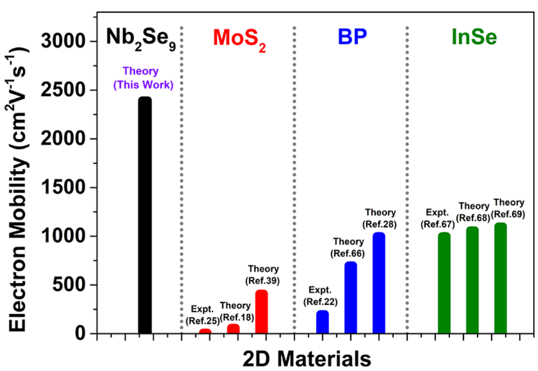

Figure 3. Electron mobilities of the Nb_2Se_9 material compared to the most studied 2D materials.

Partial Charge Density & Orbital Analysis. The band-decomposed partial charge densities of the corresponding bands near the Fermi level of the Nb_2Se_9 1D_SN, 2D_(010) plane, and 3D_bulk structures are shown in Figure 4a−f. The iso-surface values of all charge densities are 0.0015 e/a_0^3 (a_0 = Bohr radius). Charge density of the CB is much denser than that of the VB in the 2D_(010) plane. In particular, bonding orbitals of Nb and Se atoms in CB for 2D_(010) plane are more diffused, and the orbital overlaps are clearly delocalized compared to those of the 1D_SN and 3D_bulk forms, resulting in an electron mobility that is much higher than the hole mobility for the 2D_(010) plane. The VB maximum (VBM) is located along the nanowire axis, and its charge distribution is primarily in the central region of the nanowire.

In addition, we investigated the projected density of states (PDOSs) of orbital for the 1D_SN, 2D_(010) plane, and 3D_bulk Nb_2Se_9 structures by re-extracting the atom-resolved information using the COHP curves implemented in the Local-Orbital-Basis Suite Toward Electronic-Structure Reconstruction (LOBSTER).[75] The orbital-PDOSs show primary charge contribution of the VB and CB. The contribution of the VB primarily originates from the *d* orbital of the Nb atoms; however, the *p* orbital of the Se atoms contributes to both the VB and CB. The dominant contributors are the Nb in-plane $4d_{x2-y2}$ and out-of-plane $4d_{xy}$ orbitals for the CB; the contribution of out-of-plane $4d_{yz}$ orbitals is dominant for the VB of the 1D_ SN, 2D_(010) plane, and 3D_bulk structures, as shown in Figure 5a−c. Orbital contributions of Se atoms are primarily from the $4p_x$ orbital in the CB for all structures, as presented in Figure 5a−c. In the CBM, Se *p* orbitals are dominant, and the 2D_(010) plane has interchain σ bonds between Se p_x orbitals on one of the Se_5 bridges and one of the Se octahedrons.[62] Therefore, the 2D_(010) plane has a more delocalized distribution than the other structures, and the interchain interactions between the Selenium ions are strongest in the 2D_(010) plane. The hybridization in the 2D_(010) plane along the *a* direction is related to the non-covalent bonding, and it is weaker than the covalent bonding in the 2D_(010) plane along the *c* direction. This weak hybridization makes the energy of VBM and CBM change smaller along *a* direction and induces the small deformation potential with less sensitivity to the applied strain. It enables the 2D_(010) plane to have the high mobility along the *a* direction. Thus, Nb_2Se_9 can be used as an appropriate material in nanoscale optoelectronic devices in the future.

■ CONCLUSIONS

We proposed a 2D-Nb_2Se_9 material as a potential candidate for use in nanoelectronic devices. The needle-like single crystal Nb_2Se_9 is composed of numerous single Nb_2Se_9 chains linked by weak vdW interactions, and the chain bundles can be easily separated by mechanical cleavage. The proposed 1D, 2D, and 3D Nb_2Se_9 structures are free from surface dangling bonds that hinder the transport properties of carriers when scaled down.

https://doi.org/10.1021/acsomega.1c03728
ACS Omega 2021, 6, 26782−26790

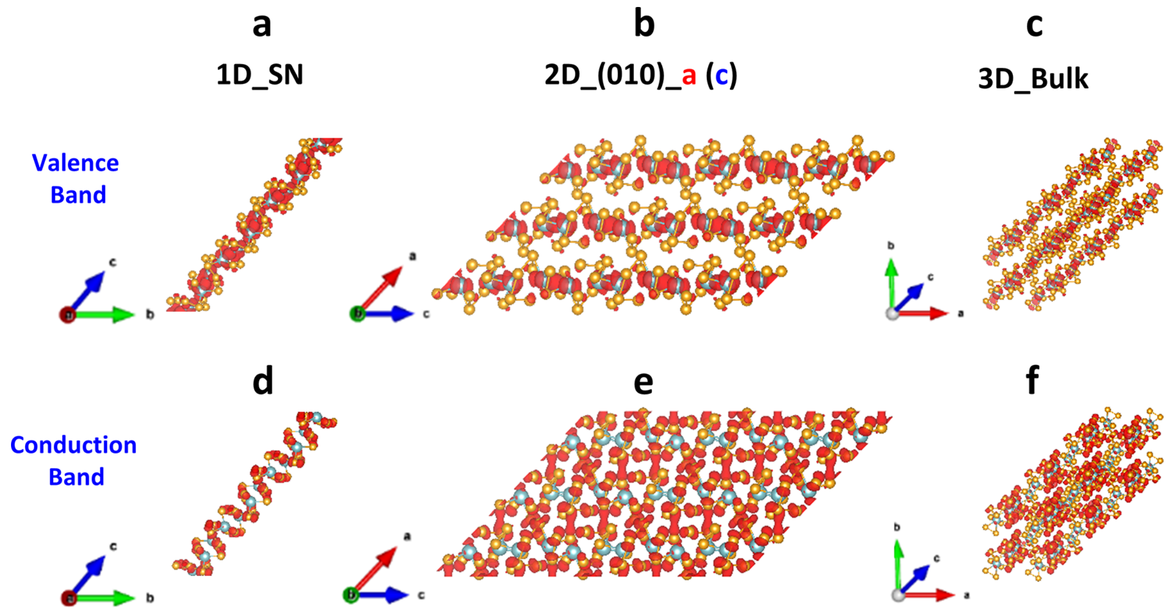

Figure 4. Side views of the band-decomposed partial charge densities of the (a, d) 1D_SN, (b, e) 2D_(010) plane, and (c, f) 3D_bulk structures of Nb_2Se_9 (upper panels (a−c) represent the VBs, whereas the lower panels (d−f) represent the CBs). Iso-surface values of all charge densities are 0.0015 e/a_0^3 (a_0 = Bohr radius).

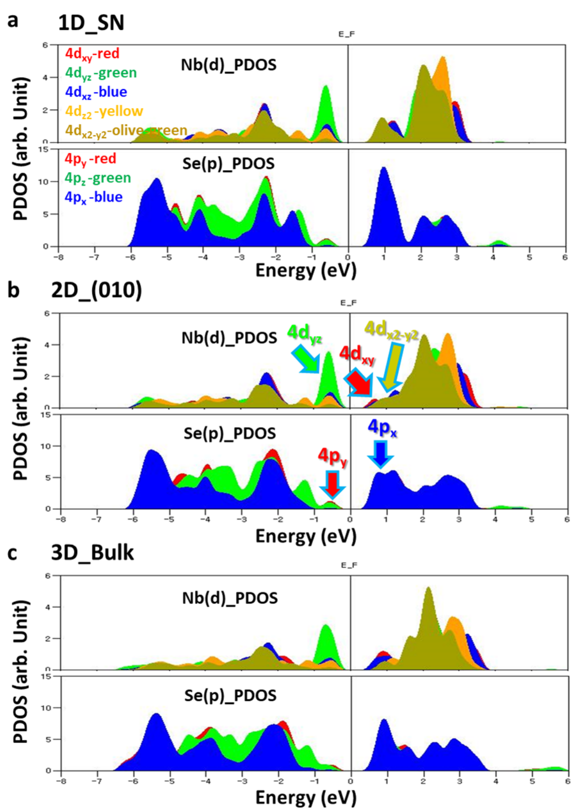

Figure 5. Orbital-PDOSs of the Nb_4d and Se_4p orbitals for the (a) 1D_SN, (b) 2D_(010) plane, and (c) 3D_bulk Nb_2Se_9 structures. (PDOSs of the $4d_{xy}$, $4d_{yz}$, $4d_{xz}$, $4d_{z^2}$, and $4d_{x^2-y^2}$ Nb orbitals are represented by red, green, blue, yellow, and olivegreen colors; contributions from the p_x, p_y, and p_z Se orbitals are represented by blue, red, and green, respectively.)

The isolated Nb_2Se_9 flakes exhibit a quasi-2D layered structure and are expected to be *p*-type semiconductors with a suitable band gap. Our transport study, based on the DP theory, predicts that electron mobility in the 2D_(010) plane along the *a* direction exhibits high values of 2.40×10^3 (HSE06) and 1.74×10^3 $cm^2\ V^{-1}\ s^{-1}$(PBE-D3), which are about 2.5−6 times higher than the highest mobilities achieved with other 2D materials, such as MoS_2, BP, and InSe at room temperature. Applying the DP theory and an anisotropic numerical formula, the high electron mobility in the 2D_(010)_*a* direction was found to originate from the smaller electron $|E_1|$ and lower effective mass in the CB, which is induced by the weaker hybridization of non-covalent bond in the 2D_(010)_*a* direction than that in the 2D_(010)_*c* direction. We also show that electron mobility of the 2D monolayered Nb_2Se_9 material is highly anisotropic ($\mu_a/\mu_c \approx 6.5$), and the anisotropy of effective mass and the deformation potential are the governing factors of the mobility anisotropy. We expect the proposed dangling-bond-free vdW Nb_2Se_9 material to be a suitable *p*-type semiconductor with high electron mobility and a nonzero band gap, with applications in optoelectronics, sensors, thermoelectric devices,[76−79] and, possibly, mid-infrared photodetectors.[27,28] However, the DP theory is based on the simplified approach so our results can give an upper limit for the mobility in Nb_2Se_9 at room temperature. The more accurate quantitative description, including other possible scattering mechanisms,[67,80−85] requires a separate consideration.

■ ASSOCIATED CONTENT

Supporting Information

The Supporting Information is available free of charge at https://pubs.acs.org/doi/10.1021/acsomega.1c03728.

Description of equations we applied for finding the primary factor that influenced the mobility anisotropy with the obtained values of various parameters for the vdW Nb_2Se_9 material, calculated using the PBE-D3 and HSE06 functionals; phonon dispersion of 2D-Nb_2Se_9; band structure using HSE06 functional for 2D-Nb_2Se_9; PDOS for the 2D-Nb_2Se_9 structure (PDF)

https://doi.org/10.1021/acsomega.1c03728
ACS Omega 2021, 6, 26782−26790

AUTHOR INFORMATION

Corresponding Authors

Jae-Young Choi − *School of Advanced Materials Science and Engineering and School of Advanced Institute of Nanotechnology, Sungkyunkwan University, Suwon 16419, Republic of Korea;* orcid.org/0000-0003-1042-6171; Email: jy.choi@skku.edu

Joonsuk Huh − *Department of Chemistry, School of Advanced Institute of Nanotechnology, and Institute of Quantum Biophysics, Sungkyunkwan University, Suwon 16419, Republic of Korea;* orcid.org/0000-0002-8792-5641; Email: joonsukhuh@skku.edu

Authors

You Kyoung Chung − *Department of Chemistry, Sungkyunkwan University, Suwon 16419, Republic of Korea*

Junho Lee − *Department of Chemistry, Sungkyunkwan University, Suwon 16419, Republic of Korea*

Weon-Gyu Lee − *Department of Chemistry, Sungkyunkwan University, Suwon 16419, Republic of Korea*

Dongchul Sung − *Department of Chemistry, Sungkyunkwan University, Suwon 16419, Republic of Korea*

Sudong Chae − *School of Advanced Materials Science and Engineering, Sungkyunkwan University, Suwon 16419, Republic of Korea*

Seungbae Oh − *School of Advanced Materials Science and Engineering, Sungkyunkwan University, Suwon 16419, Republic of Korea*

Kyung Hwan Choi − *School of Advanced Institute of Nanotechnology, Sungkyunkwan University, Suwon 16419, Republic of Korea*

Bum Jun Kim − *School of Advanced Institute of Nanotechnology, Sungkyunkwan University, Suwon 16419, Republic of Korea*

Complete contact information is available at: https://pubs.acs.org/10.1021/acsomega.1c03728

Author Contributions

J.Y.C. and J.H. directed and designed the project. Y.K.C., W.G.L., J.L., and D.S. conducted the computational studies, analyzed the data, and prepared the manuscript. S.C., S.O., K.H.C., and B.J.K. carried out the experiments and analyzed the data. All the authors have commented on this paper.

Notes

The authors declare no competing financial interest.

ACKNOWLEDGMENTS

The authors appreciate Prof. Euy Heon Hwang for the insightful discussions. This study was supported by the National Research Foundation (NRF) of Korea, grant-funded by the Korean government (MSIP) (NRF-2020R1A6A3A01100092, NRF-2019R1A6A1A10073079, NRF-2017R1A4A1015770, NRF-2021R1F1A1053283, NRF-2019M3E4A1080227, NRF-2020R1A2C2010984). J.H. acknowledges the support of the POSCO Science Fellowship of POSCO TJ Park Foundation.

ABBREVIATIONS

2D, two dimensional; DFT, density functional theory; DP, deformation potential; vdW, van der Waals; MoS_2, molybdenum disulfide; $MoSe_2$, molybdenum diselenide; WS_2, tungsten disulfide; BP, black phosphorous; FETs, field-effect transistors; mid-IR, mid-infrared; 1D, one dimensional; SN, single nanowire; VASP, Vienna ab-initio simulation package; PBE, Perdew−Burke−Ernzerhof; GGA, generalized gradient approximation; HSE, Heyd−Scuseria−Ernzerhof; COHP, crystal orbital Hamiltonian population; VB, valence band; CB, conduction band; VBM, valence band maximum; CBM, conduction band minimum; LOBSTER, Local-Orbital-Basis Suite Toward Electronic-Structure Reconstruction

REFERENCES

(1) Novoselov, K. S.; Geim, A. K.; Morozov, S. V.; Jiang, D.; Zhang, Y.; Dubonos, S. V.; Grigorieva, I. V.; Firsov, A. A. Electric Field Effect in Atomically Thin Carbon Films. *Science* **2004**, *306*, 666.

(2) Novoselov, K. S.; Geim, A. K.; Morozov, S. V.; Jiang, D.; Katsnelson, M. I.; Grigorieva, I. V.; Dubonos, S. V.; Firsov, A. A. Two-dimensional gas of massless Dirac fermions in graphene. *Nature* **2005**, *438*, 197.

(3) Bolotin, K. I.; Sikes, K. J.; Jiang, Z.; Klima, M.; Fudenberg, G.; Hone, J.; Kim, P.; Stormer, H. L. Ultrahigh electron mobility in suspended graphene. *Solid State Commun.* **2008**, *146*, 351−355.

(4) Morozov, S. V.; Novoselov, K. S.; Katsnelson, M. I.; Schedin, F.; Elias, D. C.; Jaszczak, J. A.; Geim, A. K. Giant Intrinsic Carrier Mobilities in Graphene and Its Bilayer. *Phys. Rev. Lett.* **2008**, *100*, No. 016602.

(5) Obradovic, B.; Kotlyar, R.; Heinz, F.; Matagne, P.; Rakshit, T.; Giles, M. D.; Stettler, M. A.; Nikonov, D. E. Analysis of graphene nanoribbons as a channel material for field-effect transistors. *Appl. Phys. Lett.* **2006**, *88*, 142102.

(6) Geim, A. K.; Novoselov, K. S. The rise of graphene. *Nat. Mater.* **2007**, *6*, 183.

(7) Li, X.; Wang, X.; Zhang, L.; Lee, S.; Dai, H. Chemically Derived, Ultrasmooth Graphene Nanoribbon Semiconductors. *Science* **2008**, *319*, 1229.

(8) Neugebauer, P.; Orlita, M.; Faugeras, C.; Barra, A. L.; Potemski, M. Publisher's Note: How Perfect Can Graphene Be? [Phys. Rev. Lett. 103, 136403 (2009)]. *Phys. Rev. Lett.* **2009**, *103*, 159902.

(9) Schwierz, F. Graphene transistors. *Nat. Nanotechnol.* **2010**, *5*, 487.

(10) Wang, J.; Zhao, R.; Yang, M.; Liu, Z.; Liu, Z. Inverse relationship between carrier mobility and bandgap in graphene. *J. Chem. Phys.* **2013**, *138*, No. 084701.

(11) Bai, H.; Zhu, Y.; Qiao, W.; Huang, Y. Structures, stabilities and electronic properties of graphdiyne nanoribbons. *RSC Adv.* **2011**, *1*, 768.

(12) Long, M.; Tang, L.; Wang, D.; Li, Y.; Shuai, Z. Electronic Structure and Carrier Mobility in Graphdiyne Sheet and Nanoribbons: Theoretical Predictions. *ACS Nano* **2011**, *5*, 2593.

(13) Mattheiss, L. F. Energy Bands for 2H-$NbSe_2$ and 2H-MoS_2. *Phys. Rev. Lett.* **1973**, *30*, 784−787.

(14) Seifert, G.; Tamuliene, J.; Gemming, S. Mo_nS_{2n+x} clusters—magic numbers and platelets. *Comput. Mater. Sci.* **2006**, *35*, 316−320.

(15) Li, T.; Galli, G. Electronic Properties of MoS_2 Nanoparticles. *J. Phys. Chem. C* **2007**, *111*, 16192−16196.

(16) Conley, H. J.; Wang, B.; Ziegler, J. I.; Haglund, R. F., Jr.; Pantelides, S. T.; Bolotin, K. I. Bandgap Engineering of Strained Monolayer and Bilayer MoS_2. *Nano Lett.* **2013**, *13*, 3626−3630.

(17) Radisavljevic, B.; Kis, A. Mobility engineering and a metal−insulator transition in monolayer MoS_2. *Nat. Mater.* **2013**, *12*, 815.

(18) Cai, Y.; Zhang, G.; Zhang, Y.-W. Polarity-Reversed Robust Carrier Mobility in Monolayer MoS_2 Nanoribbons. *J. Am. Chem. Soc.* **2014**, *136*, 6269.

(19) Xiao, J.; Long, M.; Li, X.; Xu, H.; Huang, H.; Gao, Y. Theoretical Prediction of Electronic Structure and Carrier Mobility in Single-walled MoS_2 Nanotubes. *Sci. Rep.* **2014**, *4*, 4327.

(20) Bromley, R. A.; Murray, R. B.; Yoffe, A. D. The band structures of some transition metal dichalcogenides III. Group VIA: trigonal prism materials. *J. Phys. C: Solid State Phys.* **1972**, *5*, 759−778.

https://doi.org/10.1021/acsomega.1c03728
ACS Omega 2021, 6, 26782−26790

(21) Houben, L.; Enyashin, A. N.; Feldman, Y.; Rosentsveig, R.; Stroppa, D. G.; Bar-Sadan, M. Diffraction from Disordered Stacking Sequences in MoS_2 and WS_2 Fullerenes and Nanotubes. *J. Phys. Chem. C* **2012**, *116*, 24350−24357.
(22) Liu, H.; Neal, A. T.; Zhu, Z.; Luo, Z.; Xu, X.; Tománek, D.; Ye, P. D. Phosphorene: An Unexplored 2D Semiconductor with a High Hole Mobility. *ACS Nano* **2014**, *8*, 4033−4041.
(23) Xiao, J.; Long, M.; Zhang, X.; Ouyang, J.; Xu, H.; Gao, Y. Theoretical predictions on the electronic structure and charge carrier mobility in 2D Phosphorus sheets. *Sci. Rep.* **2015**, *5*, 9961.
(24) Trushkov, Y.; Perebeinos, V. Phonon-limited carrier mobility in monolayer black phosphorus. *Phys. Rev. B* **2017**, *95*, No. 075436.
(25) Kaasbjerg, K.; Thygesen, K. S.; Jacobsen, K. W. Phonon-limited mobility in n-type single-layer MoS_2 from first principles. *Phys. Rev. B* **2012**, *85*, 115317.
(26) Li, L.; Engel, M.; Farmer, D. B.; Han, S.-j.; Wong, H. S. P. High-Performance p-Type Black Phosphorus Transistor with Scandium Contact. *ACS Nano* **2016**, *10*, 4672−4677.
(27) Chen, X.; Lu, X.; Deng, B.; Sinai, O.; Shao, Y.; Li, C.; Yuan, S.; Tran, V.; Watanabe, K.; Taniguchi, T.; Naveh, D.; Yang, L.; Xia, F. Widely tunable black phosphorus mid-infrared photodetector. *Nat. Commun.* **2017**, *8*, 1672.
(28) Zhao, Y.; Qiao, J.; Yu, Z.; Yu, P.; Xu, K.; Lau, S. P.; Zhou, W.; Liu, Z.; Wang, X.; Ji, W.; Chai, Y. High-Electron-Mobility and Air-Stable 2D Layered PtSe2 FETs. *Adv. Mater.* **2017**, *29*, 1604230.
(29) Island, J. O.; Steele, G. A.; Zant, H. S. J. v. d.; Castellanos-Gomez, A.; Castellanos-Gomez, A. Environmental instability of few-layer black phosphorus. *2D Mater.* **2015**, *2*, No. 011002.
(30) Castellanos-Gomez, A.; Vicarelli, L.; Prada, E.; Island, J. O.; Narasimha-Acharya, K. L.; Blanter, S. I.; Groenendijk, D. J.; Buscema, M.; Steele, G. A.; Alvarez, J. V.; Zandbergen, H. W.; Palacios, J. J.; van der Zant, H. S. J. Isolation and characterization of few-layer black phosphorus. *2D Mater.* **2014**, *1*, No. 025001.
(31) Schäfer, H., *Chemical transport reactions*. Elsevier: 2016.
(32) Tan, C.; Cao, X.; Wu, X.-J.; He, Q.; Yang, J.; Zhang, X.; Chen, J.; Zhao, W.; Han, S.; Nam, G.-H.; Sindoro, M.; Zhang, H. Recent Advances in Ultrathin Two-Dimensional Nanomaterials. *Chem. Rev.* **2017**, *117*, 6225.
(33) Lin, Z.; McCreary, A.; Briggs, N.; Subramanian, S.; Zhang, K.; Sun, Y.; Li, X.; Borys, N. J.; Yuan, H.; Fullerton-Shirey, S. K.; Chernikov, A.; Zhao, H.; McDonnell, S.; Lindenberg, A. M.; Xiao, K.; LeRoy, B. J.; Drndić, M.; Hwang, J. C. M.; Park, J.; Chhowalla, M.; Schaak, R. E.; Javey, A.; Hersam, M. C.; Robinson, J.; Terrones, M. 2D materials advances: from large scale synthesis and controlled heterostructures to improved characterization techniques, defects and applications. *2D Mater.* **2016**, *3*, No. 042001.
(34) Kim, B. J.; Jeong, B. J.; Oh, S.; Chae, S.; Choi, K. H.; Nasir, T.; Lee, S. H.; Kim, K.-W.; Lim, H. K.; Choi, I. J.; Chi, L.; Hyun, S.-H.; Yu, H. K.; Lee, J.-H.; Choi, J.-Y. Mechanical exfoliation and electrical characterization of a one-dimensional Nb2Se9 atomic crystal. *RSC Adv.* **2018**, *8*, 37724−37728.
(35) Chae, S.; Siddiqa, A. J.; Oh, S.; Kim, B. J.; Choi, K. H.; Yu, H. K.; Choi, J.-Y. Design of dispersant for highly concentrated one-dimensional Nb_2Se_9 inorganic molecular chains from bulk crystal. *Sci. Rep.* **2019**, *9*, 14579.
(36) Novoselov, K. S.; Jiang, D.; Schedin, F.; Booth, T. J.; Khotkevich, V. V.; Morozov, S. V.; Geim, A. K. Two-dimensional atomic crystals. *Proc. Natl. Acad. Sci. U. S. A.* **2005**, *102*, 10451.
(37) Chae, S.; Siddiqa, A.; Oh, S.; Kim, B.; Choi, K.; Jang, W.-S.; Kim, Y.-M.; Yu, H.; Choi, J.-Y. Isolation of Nb2Se9 Molecular Chain from Bulk One-Dimensional Crystal by Liquid Exfoliation. *Nanomaterials* **2018**, *8*, 794.
(38) Chae, S.; Oh, S.; Choi, K. H.; Lee, J. W.; Jeon, J.; Liu, Z.; Wang, C.; Lim, C.; Dong, X.; Woo, C.; Asghar, G.; Shi, L.; Kang, J.; Kim, S. J.; Song, S. Y.; Lee, J. H.; Yu, H. K.; Choi, J.-Y. A study on the bio-applicability of aqueous-dispersed van der Waals 1-D material Nb(2)Se(9) using poloxamer. *Sci. Rep.* **2021**, *11*, 176−176.
(39) Agyapong-Fordjour, F. O.-T.; Oh, S.; Lee, J.; Chae, S.; Choi, K. H.; Choi, S. H.; Boandoh, S.; Yang, W.; Huh, J.; Kim, K. K.; Choi, J. Y. One-dimensional single-chain Nb2Se9 as efficient electrocatalyst for hydrogen evolution reaction. *ACS Appl. Energy Mater.* **2019**, *2*, 5785−5792.
(40) Lee, W.-G.; Chae, S.; Chung, Y. K.; Oh, S.; Choi, J.-Y.; Huh, J. New One-Dimensional Material Nb_2Se_9: Theoretical Prediction of Indirect to Direct Band Gap Transition due to Dimensional Reduction. *Phys. Status Solidi-R* **2019**, *13*, 1800517.
(41) Island, J. O.; Molina-Mendoza, A. J.; Barawi, M.; Biele, R.; Flores, E.; Clamagirand, J. M.; Ares, J. R.; Sanchez, C.; van der Zant, H. S. J.; D'Agosta, R.; Ferrer, I. J.; Castellanos-Gomez, A. Electronics and optoelectronics of quasi-1D layered transition metal trichalcogenides. *2d Materials* **2017**, *4*, No. 022003.
(42) Radisavljevic, B.; Radenovic, A.; Brivio, J.; Giacometti, V.; Kis, A. Single-layer MoS_2 transistors. *Nat. Nanotechnol.* **2011**, *6*, 147.
(43) Liu, H.; Neal, A. T.; Ye, P. D. Channel Length Scaling of MoS_2 MOSFETs. *ACS Nano* **2012**, *6*, 8563.
(44) Lin, M.-W.; Kravchenko, I. I.; Fowlkes, J.; Li, X.; Puretzky, A. A.; Rouleau, C. M.; Geohegan, D. B.; Xiao, K. Thickness-dependent charge transport in few-layer MoS_2 field-effect transistors. *Nanotechnology* **2016**, *27*, 165203.
(45) Shafique, A.; Shin, Y.-H. Thermoelectric and phonon transport properties of two-dimensional IV−VI compounds. *Sci. Rep.* **2017**, *7*, 506.
(46) Zhang, Q.; Liu, C.; Liu, X.; Liu, J.; Cui, Z.; Zhang, Y.; Yang, L.; Zhao, Y.; Xu, T. T.; Chen, Y.; Wei, J.; Mao, Z.; Li, D. Thermal Transport in Quasi-1D van der Waals Crystal Ta2Pd3Se8 Nanowires: Size and Length Dependence. *ACS Nano* **2018**, *12*, 2634−2642.
(47) Zhao, M.; Kim, D.; Nguyen, V. L.; Jiang, J.; Sun, L.; Lee, Y. H.; Yang, H. Coherent Thermoelectric Power from Graphene Quantum Dots. *Nano Lett.* **2019**, *19*, 61−68.
(48) Bardeen, J.; Shockley, W. Deformation Potentials and Mobilities in Non-Polar Crystals. *Phys. Rev.* **1950**, *80*, 72.
(49) Tang, L.; Long, M.; Wang, D.; Shuai, Z. The role of acoustic phonon scattering in charge transport in organic semiconductors: a first-principles deformation-potential study. *Sci. China, Ser. B: Chem.* **2009**, *52*, 1646.
(50) Tahir, M.; Schwingenschlögl, U. Valley polarized quantum Hall effect and topological insulator phase transitions in silicene. *Sci. Rep.* **2013**, *3*, 1075.
(51) Beleznay, F. B.; Bogár, F.; Ladik, J. Charge carrier mobility in quasi-one-dimensional systems: Application to a guanine stack. *J. Chem. Phys.* **2003**, *119*, 5690.
(52) Alkan, M.; Yavuz, I. Intrinsic charge-mobility in benzothieno-[3,2-b][1]benzothiophene (BTBT) organic semiconductors is enhanced with long alkyl side-chains. *Phys. Chem. Chem. Phys.* **2018**, *20*, 15970.
(53) Xi, J.; Long, M.; Tang, L.; Wang, D.; Shuai, Z. First-principles prediction of charge mobility in carbon and organic nanomaterials. *Nanoscale* **2012**, *4*, 4348.
(54) Kawaji, S. The Two-Dimensional Lattice Scattering Mobility in a Semiconductor Inversion Layer. *J. Phys. Soc. Jpn.* **1969**, *27*, 906−908.
(55) Masaki, K.; Hamaguchi, C.; Taniguchi, K.; Iwase, M. Electron Mobility in Si Inversion Layers. *Jpn. J. Appl. Phys.* **1989**, *28* (Part 1, No. 10), 1856−1863.
(56) Kresse, G.; Joubert, D. From ultrasoft pseudopotentials to the projector augmented-wave method. *Phys. Rev. B* **1999**, *59*, 1758.
(57) Kresse, G.; Furthmüller, J. Efficient iterative schemes for ab initio total-energy calculations using a plane-wave basis set. *Phys. Rev. B* **1996**, *54*, 11169.
(58) Perdew, J. P.; Burke, K.; Ernzerhof, M. Generalized Gradient Approximation Made Simple. *Phys. Rev. Lett.* **1996**, *77*, 3865.
(59) Heyd, J.; Scuseria, G. E.; Ernzerhof, M. Hybrid functionals based on a screened Coulomb potential. *J. Chem. Phys.* **2003**, *118*, 8207−8215.
(60) Deringer, V. L.; Tchougréeff, A. L.; Dronskowski, R. Crystal Orbital Hamilton Population (COHP) Analysis As Projected from Plane-Wave Basis Sets. *J. Phys. Chem. A* **2011**, *115*, 5461−5466.

https://doi.org/10.1021/acsomega.1c03728
ACS Omega 2021, 6, 26782−26790

(61) Dronskowski, R.; Bloechl, P. E. Crystal orbital Hamilton populations (COHP): energy-resolved visualization of chemical bonding in solids based on density-functional calculations. *J. Phys. Chem.* **1993**, *97*, 8617−8624.
(62) Lee, W.-G.; Chung, Y. K.; Lee, J.; Kim, B. J.; Chae, S.; Jeong, B. J.; Choi, J.-Y.; Huh, J. Edge Defect-Free Anisotropic Two-Dimensional Sheets with Nearly Direct Band Gaps from a True One-Dimensional Van der Waals Nb_2Se_9 Material. *ACS Omega* **2020**, *5*, 10800−10807.
(63) Ramzan, M. S.; Bacic, V.; Jing, Y.; Kuc, A. Electronic Properties of a New Family of Layered Materials from Groups 14 and 15: First-Principles Simulations. *J. Phys. Chem. C* **2019**, *123*, 25470−25476.
(64) Gary, S. P.; Tokar, R. L. The electron-acoustic mode. *The Physics of Fluids* **1985**, *28*, 2439−2441.
(65) Bescond, M., 6 - Quantum transport in semiconductor nanowires. In *Semiconductor Nanowires*, Arbiol, J.; Xiong, Q., Eds. Woodhead Publishing: 2015; pp. 173−202, DOI: 10.1016/B978-1-78242-253-2.00006-2.
(66) Xiao, J.; Long, M.; Zhang, X.; Zhang, D.; Xu, H.; Chan, K. S. First-Principles Prediction of the Charge Mobility in Black Phosphorus Semiconductor Nanoribbons. *J. Phys. Chem. Lett.* **2015**, *6*, 4141−4147.
(67) Rudenko, A. N.; Brener, S.; Katsnelson, M. I. Intrinsic Charge Carrier Mobility in Single-Layer Black Phosphorus. *Phys. Rev. Lett.* **2016**, *116*, 246401.
(68) Bandurin, D. A.; Tyurnina, A. V.; Yu, G. L.; Mishchenko, A.; Zólyomi, V.; Morozov, S. V.; Kumar, R. K.; Gorbachev, R. V.; Kudrynskyi, Z. R.; Pezzini, S.; Kovalyuk, Z. D.; Zeitler, U.; Novoselov, K. S.; Patanè, A.; Eaves, L.; Grigorieva, I. V.; Fal'ko, V. I.; Geim, A. K.; Cao, Y. High electron mobility, quantum Hall effect and anomalous optical response in atomically thin InSe. *Nat. Nanotechnol.* **2017**, *12*, 223−227.
(69) Shi, L.-B.; Cao, S.; Yang, M.; You, Q.; Zhang, K.-C.; Bao, Y.; Zhang, Y.-J.; Niu, Y.-Y.; Qian, P. Theoretical prediction of intrinsic electron mobility of monolayer InSe: first-principles calculation. *J. Phys.: Conden. Matt.* **2019**, *32*, No. 065306.
(70) Sen, R.; Jatkar, K.; Johari, P. Modulation of electronic and transport properties of bilayer heterostructures: $InSe/MoS_2$ and InSe/h-BN as the prototype. *Phys. Rev. B* **2020**, *101*, 235425.
(71) Welser, J.; Hoyt, J.; Takagi, S.; Gibbons, J. Strain dependence of the performance enhancement in strained-Si n-MOSFETs. *Proceedings of 1994 IEEE International Electron Devices Meeting* **1994**, 373−376.
(72) Chu, M.; Sun, Y.; Aghoram, U.; Thompson, S. E. Strain: A Solution for Higher Carrier Mobility in Nanoscale MOSFETs. *Annu. Rev. Mater. Res.* **2009**, *39*, 203−229.
(73) Tsague, H. D.; Twala, B. INVESTIGATION OF CARRIER MOBILITY DEGRADATION EFFECTS ON MOSFET LEAKAGE SIMULATIONS. *International Journal of Computing* **2016**, *15*, 237−247.
(74) Veselov, D. A.; Shashkin, I. S.; Bakhvalov, K. V.; Lyutetskiy, A. V.; Pikhtin, N. A.; Rastegaeva, M. G.; Slipchenko, S. O.; Bechvay, E. A.; Strelets, V. A.; Shamakhov, V. V.; Tarasov, I. S. On the problem of internal optical loss and current leakage in laser heterostructures based on AlGaInAs/InP solid solutions. *Semiconductors* **2016**, *50*, 1225−1230.
(75) Maintz, S.; Deringer, V. L.; Tchougréeff, A. L.; Dronskowski, R. LOBSTER: A tool to extract chemical bonding from plane-wave based DFT. *J. Comput. Chem.* **2016**, *37*, 1030.
(76) Golden, J. H.; DiSalvo, F. J.; Fréchet, J. M. J.; Silcox, J.; Thomas, M.; Elman, J. Subnanometer-Diameter Wires Isolated in a Polymer Matrix by Fast Polymerization. *Science* **1996**, *273*, 782.
(77) Qi, X.; Osterloh, F. E. Chemical Sensing with $LiMo_3Se_3$ Nanowire Films. *J. Am. Chem. Soc.* **2005**, *127*, 7666.
(78) Allen, M.; Sabio, E. M.; Qi, X.; Nwengela, B.; Islam, M. S.; Osterloh, F. E. Metallic $LiMo_3Se_3$ Nanowire Film Sensors for Electrical Detection of Metal Ions in Water. *Langmuir* **2008**, *24*, 7031.
(79) Amani, M.; Tan, C.; Zhang, G.; Zhao, C.; Bullock, J.; Song, X.; Kim, H.; Shrestha, V. R.; Gao, Y.; Crozier, K. B.; Scott, M.; Javey, A. Solution-Synthesized High-Mobility Tellurium Nanoflakes for Short-Wave Infrared Photodetectors. *ACS Nano* **2018**, *12*, 7253−7263.
(80) Mariani, E.; von Oppen, F. Flexural Phonons in Free-Standing Graphene. *Phys. Rev. Lett.* **2008**, *100*, No. 076801.
(81) Kioseoglou, G.; Hanbicki, A. T.; Currie, M.; Friedman, A. L.; Jonker, B. T. Optical polarization and intervalley scattering in single layers of MoS2 and MoSe2. *Sci. Rep.* **2016**, *6*, 25041.
(82) Rodrigues, J. N. B. Intervalley scattering of graphene massless Dirac fermions at 3-periodic grain boundaries. *Phys. Rev. B* **2016**, *94*, 134201.
(83) Zhou, J.; Cheng, S.; You, W.-L.; Jiang, H. Effects of intervalley scattering on the transport properties in one−dimensional valleytronic devices. *Sci. Rep.* **2016**, *6*, 23211.
(84) Carvalho, B. R.; Wang, Y.; Mignuzzi, S.; Roy, D.; Terrones, M.; Fantini, C.; Crespi, V. H.; Malard, L. M.; Pimenta, M. A. Intervalley scattering by acoustic phonons in two-dimensional MoS2 revealed by double-resonance Raman spectroscopy. *Nat. Commun.* **2017**, *8*, 14670.
(85) Zhao, W. L. Z.; Tikhonov, K. S.; Finkel'stein, A. M. Flexural phonons in supported graphene: from pinning to localization. *Sci. Rep.* **2018**, *8*, 16256.

https://doi.org/10.1021/acsomega.1c03728
ACS Omega 2021, 6, 26782−26790